The Tumor Suppressor Death-Associated Protein Kinase Targets to TCR-Stimulated NF-κB Activation[1]

Ya-Ting Chuang,*‡ Li-Wen Fang,‡¶ Ming-Hsien Lin-Feng,‡ Ruey-Hwa Chen,†§ and Ming-Zong Lai[2]*‡

Death-associated protein kinase (DAPK) is a unique multidomain kinase acting both as a tumor suppressor and an apoptosis inducer. The molecular mechanism underlying the effector function of DAPK is not fully understood, while the role of DAPK in T lymphocyte activation is mostly unknown. DAPK was activated after TCR stimulation. Through the expression of a dominant-negative and a constitutively active form of DAPK in T cells, we found that DAPK negatively regulated T cell activation. DAPK markedly affected T cell proliferation and IL-2 production. We identified TCR-induced NF-κB activation as a target of DAPK. In contrast, IL-1β- and TNF-α-triggered NF-κB activation was not affected by DAPK. We further found that DAPK selectively modulated the TCR-induced translocation of protein kinase Cθ, Bcl-10, and IκB kinase into membrane rafts. Notably, the effect of DAPK on the raft entry was specific for the NF-κB pathway, as other raft-associated molecules, such as linker for activation of T cells, were not affected. Our results clearly demonstrate that DAPK is a novel regulator targeted to TCR-activated NF-κB and T cell activation. ***The Journal of Immunology,*** **2008, 180: 3238–3249.**

Death-associated protein kinase (DAPK)[3] is a multidomain 160-kDa calcium/calmodulin-regulated Ser/Thr kinase (1–3). The kinase domain is located at the N terminus, followed by a calcium/calmodulin regulatory segment, ankyrin repeats, and a cytoskeleton-binding region. A death domain is situated near the C-terminal end of DAPK. In the resting state, the calcium/calmodulin regulatory sequence interacts with the peptide-binding site of the catalytic subunit and prevents substrate binding. Calcium-activated calmodulin removes this inhibitory self-association, and thus deletion of the calcium/calmodulin regulatory segment converts DAPK into a constitutively active kinase (4). On the contrary, alanine mutation of the key lysine residue in the kinase domain to alanine (K42A) nullifies kinase activity, and [K42A]DAPK acts as a dominant-negative (DN) form (4).

DAPK is a well-known tumor suppressor (2). Part of this tumor-suppressing activity by DAPK could be attributed to the sensitization of cancer cells to apoptosis. DAPK has been shown to participate in many different types of cell death, such as IFN-γ-induced cell death (5), TNF-α- and Fas-triggered apoptosis (6), TGF-β-induced cell death (7), ceramide-mediated apoptosis (8, 9), matrix detachment-induced apoptosis (10), autophagic cell death (11), neurotoxin-induced apoptosis (12), netrin-1 receptor uncoordinated protein 5 homolog 2 (UNC5H2)-mediated apoptosis (13), and ERK-triggered cell death (14).

The molecular mechanism underlying the proapoptotic function of DAPK is not fully understood, but it is believed that the death domain of DAPK may contribute to this activity (6, 15). Up-regulation of p53 is seen in some models of DAPK-induced cell death (16). The proapoptotic activity of DAPK is also linked to an interaction with actin cytoskeleton (4). Autophage vesicle formation, death-associated morphological change, and stress fiber formation involve DAPK-induced phosphorylation of myosin II regulatory L chain (MLC) (3, 4, 17–19). MLC is also phosphorylated by zipper-interacting protein kinase, the kinase activated by DAPK (10, 20). In addition, DAPK inhibits integrin activity and cell adhesion (10, 21). DAPK may also act as a sensor for mitochondrial membrane potential (12). At the signaling level, there is an interesting cross-talk between DAPK and ERK in the regulation of apoptosis. DAPK enhances ERK retention in the cytoplasm to reduce nuclear signaling of ERK (22). The phosphorylation of DAPK by p90 ribosomal S6 kinase, a kinase downstream of ERK, leads to reduced DAPK apoptotic activity (23).

NF-κB is a potent antiapoptotic transcription factor (24). NF-κB induces the expression of several key survival gene products including cellular inhibitors of apoptosis (c-IAPs), X chromosome-linked IAP, cellular FLIP, A1, Bcl-x_L, growth arrest and DNA damage-45β, and TNFR-associated factors 1 and 2. Perceivably, inhibition of NF-κB enhances apoptosis induction at various stages of apoptotic cascade. NF-κB is also an essential survival factor for T lymphocytes (25–27). The processes from TCR engagement to NF-κB activation involves phosphorylation of protein kinase Cθ (PKCθ), assembly of CARD-containing membrane associated guanylate kinase protein 1, Bcl-10, and mucosa-associated lymphoid-tissue lymphoma translocation gene 1 (MALT1) trimolecule complex, and activation of the IκB kinase (IKK) complex (28–31),

*Institute of Immunology and †Institute of Molecular Medicine, College of Medicine, National Taiwan University, Taipei, Taiwan; ‡Institute of Molecular Biology and §Institute of Biological Chemistry, Academia Sinica, Taipei, Taiwan; and ¶Department of Medical Nutrition, I-Shou University, Kaoshiung, Taiwan, Republic of China

Received for publication November 18, 2007. Accepted for publication December 25, 2007.

The costs of publication of this article were defrayed in part by the payment of page charges. This article must therefore be hereby marked *advertisement* in accordance with 18 U.S.C. Section 1734 solely to indicate this fact.

[1] This work was supported by Grant AS-95-TP-B01 from Academia Sinica (Taipei, Taiwan) and Grant NHRI-EX96-9527NI from NHRI (Miadi, Taiwan).

[2] Address correspondence and reprint requests to Dr. Ming-Zong Lai, Institute of Molecular Biology, Academia Sinica, Nankang, Taipei 11529, Taiwan. E-mail address: mblai@imb.sinica.edu.tw

[3] Abbreviations used in this paper: DAPK, death-associated protein kinase; MLC, myosin II regulatory L chain; c-IAP, cellular inhibitor of apoptosis; IKK, IκB kinase; PKC, protein kinase C; siRNA, small interfering RNA; MALT1, mucosa-associated lymphoid-tissue lymphoma translocation gene 1; LAT, linker for activation of T cells; Hsp, heat shock protein; YFP, yellow fluorescent protein; DRAK, DAPK-related associated kinase; DN, dominant negative; NLC, normal littermate control; CHX, cycloheximide.

even though the fine molecular mechanisms are still being unveiled (32, 33). The TCR-induced NF-κB activation cascade is distinct from NF-κB activation pathways downstream of TNFRI, IL-1R, or TLR (27, 34, 35). In the present study, we examined the regulatory role of DAPK in T cell activation. We mapped one of the targets suppressed by DAPK in T cells to NF-κB. In addition, DAPK selectively inhibited TCR-induced, but not TNF-α- or IL-1β-triggered, NF-κB activation. As a consequence of the specific inhibition on NF-κB by DAPK, blockage of DAPK activity led to greatly enhanced T cell activation. Our results reveal a novel role of tumor suppressor DAPK in TCR-induced NF-κB activation.

Materials and Methods

T cell culture and retroviral infection

Human T cells were isolated from peripheral blood by the RosetteSep Human T Cell Enrichment mixture (StemCell Technologies) according to the suggested protocol. The purity of $CD3^+$ T cells was over 97% as determined by FACS analysis. DO11.10 cells are T cell hybridoma specific for $OVA_{323–339}$ in the context of $I\text{-}A^d$ (36). All T cells were cultured in RPMI 1640 medium with 10% FCS (Invitrogen Life Technologies), 10 mM glutamine, 100 U/ml penicillin, 100 μg/ml streptomycin, and 2×10^{-5} M 2-ME. Apoptosis was quantitated by propidium iodide staining (37). A fraction of cells with $subG_1$ DNA content was determined using the CELLFIT software program on a FACScan (BD Biosciences).

Wild-type DAPK, [K42A]DAPK, [ΔCAM]DAPK were subcloned into pGC-IRES-yellow fluorescent protein (YFP), a homolog of pGC-IRES-GFP (a gift from Dr. G. Costa, Stanford University, Stanford, CA) to generate pGC-DAPK-IRES-YFP, pGC-[K42A]DAPK-IRES-YFP, and pGC-[ΔCAM]DAPK-IRES-YFP. Retroviruses were generated by transfection of Phoenix cells (gifts of Dr. G. P. Nolan, Stanford University) with 10 μg of pGC-YFP or pGC-DAPK-YFP plasmids. Phoenix cell supernatants containing retrovirus were collected 48 h after transfection. Viral titers were determined using NIH 3T3 cells, and virus stocks with titers $>1 \times 10^6$ were used for spin infection of DO11.10 T cell hybridoma or Jurkat-Eco T cells. Forty-eight hours after infection, YFP-expressing DO11.10 cells were isolated by sorting on FACSVantage SE (BD Biosciences).

Small interfering RNA (siRNA)

Oligonucleotides corresponding to the DAPK-specific siRNA sequence were subcloned into pSUPER.retro vector (Oligoengene) with both neo and GFP genes. Retrovirus were packed in 293T cells and used to infect DO11.10 or Jurkat cells. Forty-eight hours after viral transduction, DO11.10 and Jurkat cells were resuspended in fresh medium containing G418 at 1 mg/ml and selected for 2 wk. G418-resistant cells were maintained in medium containing 500 μg/ml puromycin and homologous GFP expression was confirmed by flow cytometry. The sequence of mouse DAPK siRNA (mDAPKsi) is: CAC CAG TAC CCT TGC CAAA, while the two sequences for human DAPK siRNA are: CAA GAA ACG TTA GCA AATG (hsi-1), GGT CAA GGA TCC AAA GAAG (hsi-2), respectively. The sequence of the control siRNA for mouse DAPK and human DAPK are CAC CAG AAC CAT GGC CAAC and GAT CAA GAA CAA GAC GCAG, respectively. The specific primers used in RT-PCR to determine mouse DAPK were: 5′: TCTGAGGATGACCTC, 3′: GCTTTGCTGGTGGAT.

Transgenic mice construction

[K42A]DAPK and [ΔCAM]DAPK were subcloned into a human CD2 cassette (38), a gift from Dr. D. Kioussis (National Institute for Medical Research, London, U.K.). Transgenic mice were generated in the Transgene/Knock-Out Core Facility (Institute of Molecular Biology, Academia Sinica, Taipei, Taiwan). CD2-[K42A]DAPK and CD2-[ΔCAM]DAPK were microinjected into the pronuclei of C57BL/6 zygotes. At least three independent founders from each construct were obtained. All transgenic mice were maintained in the specific pathogen-free mice facility of the Institute of Molecular Biology, Academia Sinica. All mouse experiments were conducted under the approval of the Experimental Animal Committee of Academia Sinica. The sequence of PCR primers to identify transgenic DAPK were: 5′: GATGCCGCAGACCTT, 3′: CAGCTCTCAAAGTCAGTG.

Nuclear extract and total cell extract

Harvested cells were lysed in 10 mM Tris-HCl (pH 7.4), 10 mM NaCl, 3 mM $MgCl_2$, and 0.5% Nonidet P-40 (Nonidet P-40). The lysates were incubated on ice for 5 min and then centrifuged at $200 \times g$ for 3 min at 4°C. The pellet (nuclei) was suspended in hypertonic buffer (20 mM HEPES (pH 7.9), 1.5 mM $MgCl_2$, 0.3 M KCl, 0.5 mM DTT, 1 mM PMSF, 20% glycerol, and 0.4 mM EDTA) and rocked at 4°C for >30 min. After centrifugation at $12,000 \times g$ for 10 min, the collected supernatant was then mixed with two volumes of hypertonic buffer (without KCl) and frozen immediately at −80°C. Total cell extract was prepared by resuspending cells in hypotonic buffer (10 mM HEPES (pH 7.9), 1.5 mM $MgCl_2$, 10 mM KCl, 0.5 mM DTT, 0.5 mM PMSF, 100 μg/ml aprotinin, and 1.25 μg/ml leupeptin) and lysing by three cycles of freezing and thawing. A one-tenth volume of 3 M KCl was then added to the lysate, rocked at 4°C for 30 min, and isolated as indicated in nuclear extract. Protein concentration was determined by Bradford assay (Bio-Rad).

Immunoblots

Cell extracts (30–50 μg) were resolved on SDS-PAGE and transferred to polyvinylidene difluoride membranes (Millipore) for 4 h at 20 V. Membranes were washed in rinse buffer (PBS with 2% Tween 20) at room temperature for 15 min and incubated in blocking buffer (5% nonfat milk in rinse buffer) for 1.5 h. The membrane was then incubated with primary Abs for 2 h at room temperature and afterward washed three times with rinse buffer. The membrane was then incubated with 1/1000 diluted HRP-conjugated goat anti-rabbit Ig or HRP-conjugated rabbit anti-mouse Ig, followed by development with ECL reagents. The Abs used were: anti-human DAPK (clone DAPK-55) and anti-phospho (S308) DAPK (clone DKPS308) (Sigma-Aldrich); anti-*myc* (clone 9E10), anti-ERK2 (C-14), NF-κB p65, Bcl-10, linker for activation of T cells (LAT), anti-MLC (Santa Cruz Biotechnology); anti-phospho (T202/Y204) ERK, anti-phospho (Y191) LAT, anti-IκBα, anti-IKKα, anti-IKKβ, anti-PKCθ, anti-phospho-PKCθ (T538), and anti-phospho-MLC (Cell Signaling). Anti-NFAT1, anti-NFAT2, and flotilin-specific Abs were purchased from BD Pharmingen. Anti-β-tubulin was obtained from Upstate Biotechnology. HRP-conjugated secondary Abs and ECL were obtained from Amersham Bioscience.

EMSA

Oligonucleotide probe was end labeled using T4 polynucleotide kinase and [γ-^{32}P]ATP. Nuclear extract (10 μg) was incubated with radiolabeled probes (0.1–0.5 ng of DNA containing 1×10^4–1.5×10^5 cpm) plus 0.5 μg of poly(dI-dC) (Pharmacia) in a total volume of 20 μl. The mixture was incubated at room temperature for 20–25 min and electrophoresed through 4–5% native polyacrylamide gel in 22.5 mM Tris-borate/0.5 mM EDTA (pH 8.0) for 3.5 h at 150 V. Gels were dried before autoradiography. Supershifting was performed by preincubating nuclear extract with 1 μg of Ab for 10 min at 4°C before probe addition. The NF-κB probe used was from Ig κ-chain, with the sequence: 5′-GAGGGGACTTTCCGAGGGGACTTTCCGAGA.

Lipid raft purification

T cells ($3\sim5 \times 10^7$) were activated with plate-bound anti-CD3 (5 μg/ml) plus anti-CD28 (2.5 μg/ml) at 37°C for 30 min and then lysed in 600 μl of MNE buffer (25 mM morpholinoethanesulfonic acid (pH 6.5), 150 mM NaCl, 5 mM EDTA, 30 mM sodium pyrophosphate, 1 mM sodium orthovanadate, 10 μg of each protease inhibitor per ml with 0.25% Triton X-100) for 15 min on ice. The cell lysates were mixed with 600 μl of 80% sucrose in MNE buffer and transferred to a Beckman Ultracentrifuge tube. A total of 2.4 ml of 30% sucrose followed by 1.2 ml of 5% sucrose in MNE buffer was overlaid. Samples were separated by ultracentrifuge in a SW55Ti rotor at $200,000 \times g$ for 20 h. Fractions (600 μl each) were collected from the top of the gradient. Analysis of each fraction by immunoblots with flotillin indicated that fractions 2–4 represented rafts, while fractions 7 and 8 were soluble fractions. Raft and soluble fractions were then pooled and separated for further analysis.

Quantitation by densitometry measurements

For densitometry measurements, the developed films were analyzed on a Luminescent Image Analyzer LAS-1000 (Fuji Photo Film) using Image Gauge software (version 3.2). Quant mode was used to select the reading area and to subtract background. In short, an area just sufficient to cover each protein band in a film was selected. The selected region was then duplicated to enclose every band, and the densitometry reading of each region was recorded. The same region was duplicated on the open area of the film and was used as the background reading for subtraction. After subtraction, the reading was then normalized against internal control (such as heat shock protein (Hsp) 70). The reading from the unstimulated control T cell samples were used as 1.

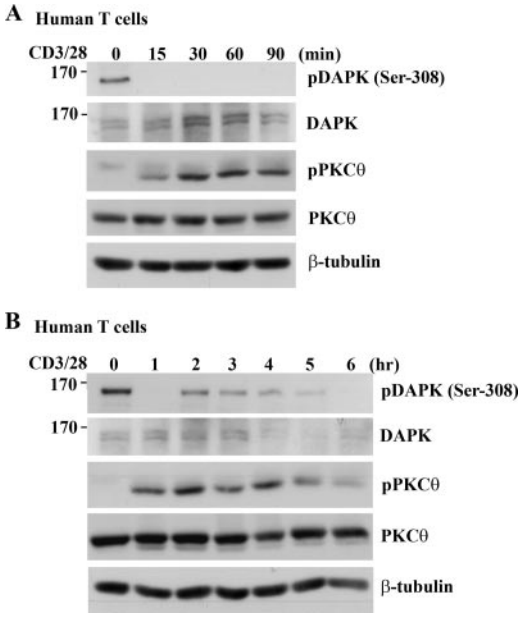

FIGURE 1. Activation and degradation of DAPK by TCR stimulation. DAPK was dephosphorylated at Ser^{308} (*A*) and degraded (*B*) followed by TCR engagement. Purified human PBL T cells were stimulated with OKT3 (5 μg/ml) and anti-CD28 (2.5 μg/ml) for 15–90 min (*A*), or 1–6 h (*B*), and total cell lysates were prepared. The contents of DAPK, phospho-Ser^{308} DAPK, phospho-PKCθ, and PKCθ were determined by specific Abs. Constitutive heat shock protein 70 was used as internal control. Molecular mass markers (in kilodaltons) were indicated to the left.

Results

DAPK is activated then degraded by TCR stimulation

DAPK is phosphorylated by itself at serine 308 to interfere with the binding of Ca^{2+}/calmodulin in resting state (39). Activation of DAPK is accompanied with dephosphorylation at serine 308, by an unidentified phosphatase, and the association of Ca^{2+}/calmodulin (3). Serine 308 dephosphorylation has been shown to indicate DAPK activation stimulated by UNC5H2, TNF-α, ceramide, or ischemia (13, 40, 41). We therefore used the dephosphorylation of DAPK at Ser^{308} to measure the activation of the endogenous DAPK after TCR stimulation. DAPK was constitutively expressed in T cells (Fig. 1*A*). In resting human T cells, DAPK was phosphorylated at serine 308, as detected by phospho-Ser^{308}-specific Ab (Fig. 1*A*). Stimulation of T cells with anti-CD3 plus anti-CD28 Abs, marked by time-dependent prominent PKCθ phosphorylation in the context of a steady PKCθ level, led to immediate dephosphorylation of DAPK. Activation of DAPK persisted until 90 min (Fig. 1*A*). This was followed by a graduate inactivation of DAPK, shown by rephosphorylation of DAPK 2 h after TCR stimulation (Fig. 1*B*). At 4 h, there was a clear reduction in the total level of DAPK (Fig. 1*B*), presumably due to DAPK degradation (40, 41). This was correlated with a proportional decrease in the extent of serine 308 phosphorylation on DAPK. The similar DAPK activation pattern was observed in another five batches of T lymphocytes. Therefore, TCR stimulation activates endogenous DAPK and eventually promotes DAPK degradation. Some small variations were found between different batches of T cell

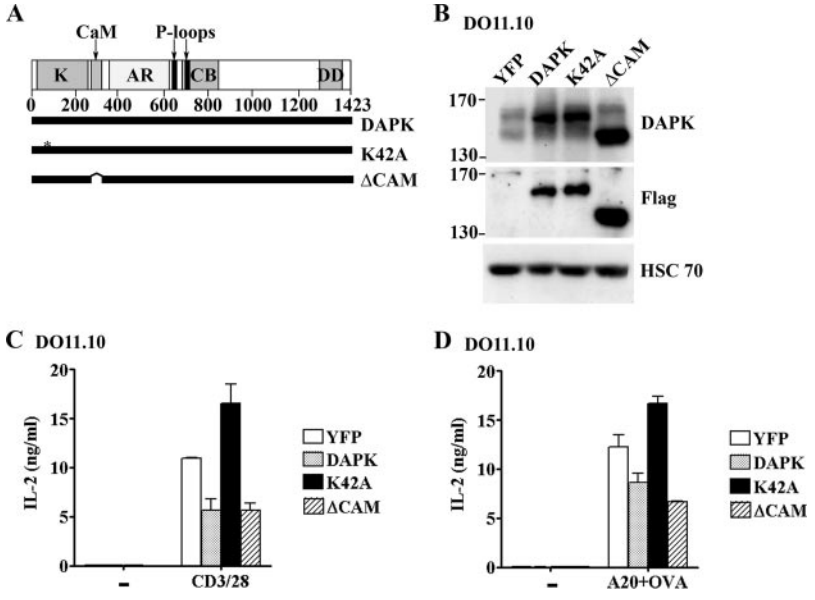

FIGURE 2. DAPK inhibits IL-2 production, while DN DAPK enhances IL-2 production in T cells. *A*, Schematic representation of DAPK and its mutants used in these studies. The various motifs and domains are: K, kinase domain; CaM, CaM-binding domain; AR, ankyrin repeats; CB, cytoskeleton-binding domain; DD, death domain. The numbers below indicate the amino acid positions. The mutation at K42A (starred) generates the DN form of DAPK, while deletion of CaM (ΔCaM) produced a DAPK with constitutively active kinase. *B*, Overexpression of DAPK and its mutants in DO11.10. DO11.10 cells were transduced with pGC-YFP, pGC-DAPK-YFP, pGC-[K42A]DAPK-YFP, and pGC-[ΔCAM]DAPK-YFP by retroviral infection. YFP-expressing T cells were sorted on a FACSVantage SE. DAPK and its mutant proteins were detected by Abs specific for human DAPK and for Flag tag. HSC70 was used as the internal control. Molecular mass markers (in kilodaltons) were indicated to the left. *C* and *D*, DAPK and [ΔCAM]DAPK inhibited T cell activation, while [K42A]DAPK increased T cell activation. Control DO11.10 T cells (YFP) and DO11.10 T cells expressing wild-type DAPK (DAPK), [K42A]DAPK (K42A), and [ΔCAM]DAPK (ΔCAM) were activated by the plate-bound anti-CD3 Ab (0.6 μg/ml) plus anti-CD28 Ab (0.3 μg/ml) (*C*), or with $OVA_{323–339}$ peptide (1.25 μg/ml) presented by A20 cells (*D*), and IL-2 production was quantitated 24 h later by IL-2-dependent cell line HT-2. Data are average of triplicate in one experiment. Error bars indicate SD. Values of *p* for YFP to DAPK, YFP to K42A, and YFP to ΔCAM were <0.05 in *C* and <0.01 in *D*. Similar results are observed in another two independent experiments.

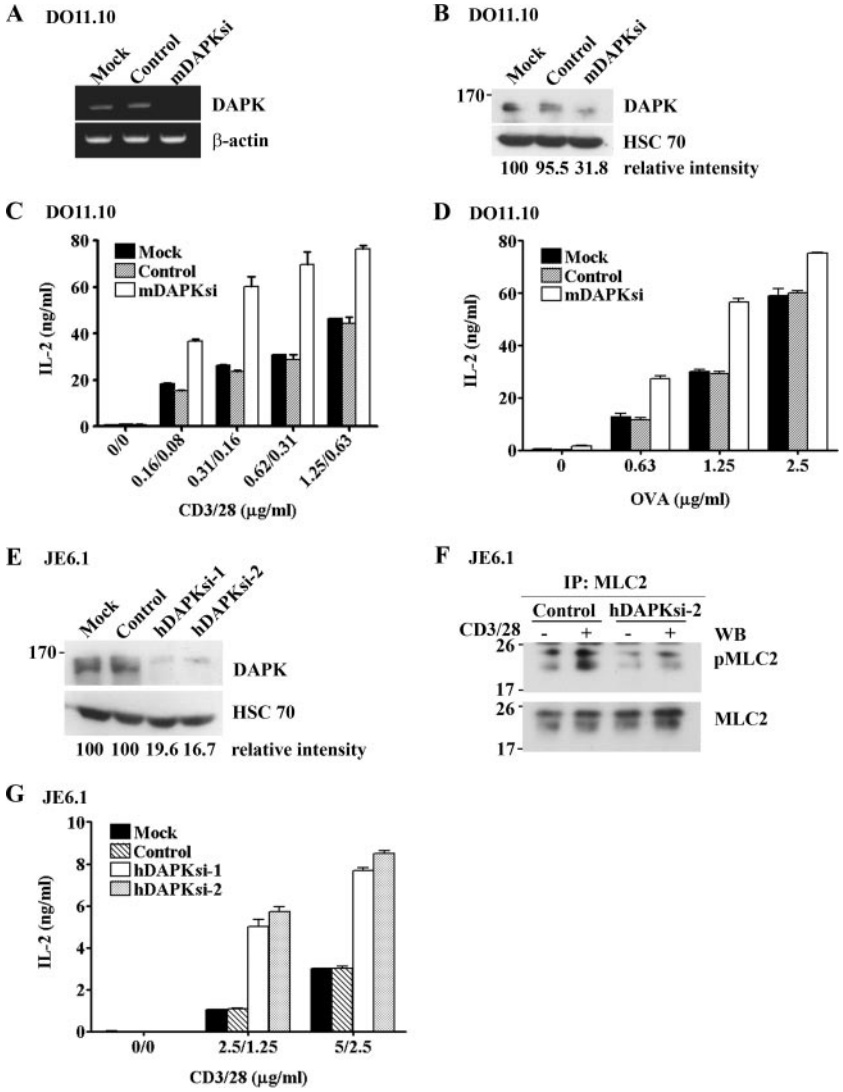

FIGURE 3. Down-regulation of the endogenous DAPK by siRNA increases T cell activation. *A* and *B*, Down-regulation of DAPK expression in DO11.10 T cells. DO11.10 cells were transduced with pSUPER.retro vector (Mock), mouse DAPK-specific siRNA-containing pSR (mDAPKsi), or mutated nonspecific siRNA (Control). The GFP-expressing population was isolated by FACS sorting. DAPK RNA levels were determined by RT-PCR using mouse DAPK-specific primers, with β-actin as the internal control (*A*). DAPK protein levels were assessed by immunoblots using DAPK-specific Abs (*B*), and were quantitated by densitometer. The relative protein levels were calculated using mock DAPK as 100. *C* and *D*, Knockdown of DAPK in DO11.10 T cells enhanced TCR-stimulated IL-2 production. Vector-transfected DO11.10 cells (Mock), nonspecific siRNA-transfected (Control), or DAPK-knockdown DO11.10 cells (mDAPKsi) were activated with immobilized anti-CD3/anti-CD28 at concentrations indicated (*C*), or with A20 cells plus $OVA_{323-339}$ peptide at concentrations indicated (*D*), and IL-2 produced was quantitated 24 h later. Data are average of triplicate in one experiment, with SD indicated by error bars. In both studies, p values between mock and mDAPKsi, or between control and mDAPKsi are <0.01, except the OVA (2.5 μg/ml) set where $p < 0.05$ between mock and mDAPKsi. *E*, Knockdown of DAPK in Jurkat cells. Jurkat cells (JE6.1) were transduced with vector alone (Mock), pSR-nonspecific siRNA (Control), pSR-human DAPK siRNA sequence 1 or 2 (hDAPKsi-1, si-2), and sorted by GFP expression. Protein contents of DAPK were determined by immunoblot using DAPK Ab and quantitated by densitometry. The relative DAPK levels were calculated using mock DAPK as 100. *F*, Reduced MLC phosphorylation in Jurkat cells with DAPK down-regulated. Control and hDAPKsi2 Jurkat cells were activated by anti-CD3/CD28 for 15 min. Cell lysates from Jurkat cells before and after activation were precipitated with anti-MLC, and contents of phospho-MLC were determined. *G*, DAPK knockdown in Jurkat T cells promoted IL-2 generation. Vector-only JE6.1 cells (Mock), nonspecific siRNA-transfected (Control), and DAPK-knockdown Jurkat cells (hDAPKsi-1 and hDAPKsi-2) were activated with anti-CD3 and -CD28 Abs immobilized at the concentration indicated, and IL-2 production was quantitated 24 h later. Data are the average of triplicate in one experiment. Error bars indicate SE. Values of p between mock and hDAPKsi-1, mock and hDAPKsi-1, control and hDAPKsi-1, or between control and hDAPKsi-2 are <0.01. Similar results are observed in another two repeated experiments.

activation. For example, inactivation of DAPK was detected as early as 60 min after TCR engagement in two experiments, while the degradation of DAPK became evident as late as 6 h in another batch of T cells. It may be noted that the small increase of DAPK detected at 30–60 min (Fig. 1*A*) was not seen in every batch of human T cells analyzed. Between different batches of experiments, there was also variation in the persistence of PKCθ phosphorylation, ranging from 4 h (Fig. 1*B*) to 7 h after TCR stimulation.

T cell activation is inhibited by active DAPK and enhanced by DN DAPK

To evaluate the functional role of DAPK in T cell activation, wild-type human DAPK, the kinase-dead DN form of DAPK

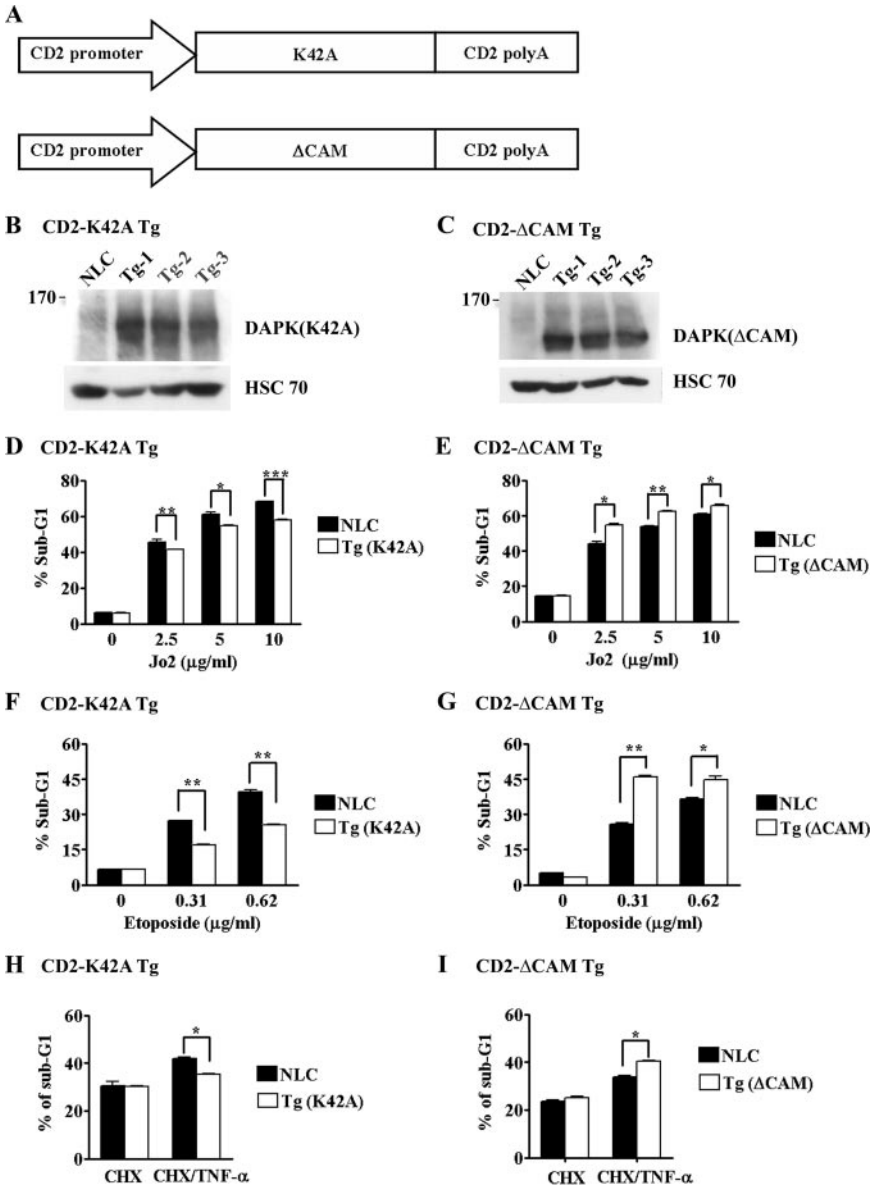

FIGURE 4. T cell-specific transgenic expression of [K42A]DAPK and [ΔCAM]DAPK. *A*, Schematic representation of the CD2-[K42A]DAPK and the CD2-[ΔCAM]DAPK transgenes. [K42A]DAPK and [ΔCAM]DAPK were subcloned into the CD2 cassette. *B*, Expression of [K42A]DAPK transgene protein in three independent lines of CD2-[K42A]DAPK-transgenic mice. Cell lysates were prepared from purified splenic T cells of three independent transgenic mouse lines (Tg-1, -2, -3) and a NLC, and the contents of DAPK were assessed by immunoblots. *C*, Expression of [ΔCAM]DAPK transgene protein in three lines of CD2-[ΔCAM]DAPK-transgenic mice. The levels of DAPK in cell lysates prepared from purified splenic T cells of a NLC mouse and three independent transgenic mouse lines (Tg-1, -2, -3) were determined by immunoblots. *D* and *F*, Fas- or etoposide-induced apoptosis was reduced in [K42A]DAPK-transgenic thymocytes. Thymocytes from CD2-[K42A]DAPK-transgenic mice and their normal littermate control were treated with Jo2 (*D*) or etoposide (*F*), and apoptosis was quantitated at 48 h (*D*) or 14 h (*F*) after treatment. *E* and *G*, Elevated Jo2- or etoposide-triggered apoptosis in [ΔCAM]DAPK-transgenic thymocytes. Thymocytes from CD2-[ΔCAM]DAPK-transgenic mice were treated with Jo2 (*E*) or etoposide (*G*) at the concentration indicated, and apoptosis was assessed. *H* and *I*, DAPK-dependent TNF-α-induced cell death. *H*, [K42A]DAPK-or, *I*, [ΔCAM]DAPK-transgenic thymocytes were treated with CHX (0.16 μg/ml) with or without TNF-α (5 ng/ml), and cell death was determined 48 h after treatment. ∗, $p < 0.05$; ∗∗, $p < 0.01$; ∗∗∗, $p < 0.001$ for paired *t* test.

(K42A, Fig. 2*A*), and the constitutively kinase active form of DAPK (ΔCAM, Fig. 2*A*) were overexpressed in DO11.10 murine T cell hybridomas. Expression of Flag-tagged human DAPK and its mutant proteins in mouse T cells was confirmed by Western blot with Abs specific for human DAPK or Flag tag (Fig. 2*B*). DO11.10 T cells were activated by the plate-bound anti-CD3/anti-CD28 Abs, and IL-2 produced was used as an indicator of integrated T cell activation. Fig. 2*C* illustrates that expression of wild-type DAPK inhibited TCR-stimulated IL-2 production, relative to the YFP control. Suppression of T cell activation was found with active form of DAPK (ΔCAM, Fig. 2*C*). In contrast, loss of DAPK activity by [K42A]DAPK increased IL-2 generation. A similar effect of these DAPK proteins on T cell activation was observed when T cells were stimulated with an antigenic peptide ($OVA_{323–339}$) presented by A20 B cells (Fig. 2*D*). These results suggest that DAPK plays an inhibitory role in T cell activation.

Down-regulation of DAPK by siRNA promotes T cell activation

In addition to DAPK, T lymphocytes express DAPK-related kinases (DRAKs; such as DRAK2) (3). To exclude the possibility that the observed stimulatory effect of [K42A]DAPK on T cell activation was due to a promiscuous inhibition of other DAPK-related kinases, we used siRNA to specifically down-regulate DAPK. Fig. 3*A* demonstrates that the expression of mouse DAPK transcripts in DO11.10 cells was knocked down by the specific siRNA (mDAPKsi), relative to vector only (Mock). The mutated mouse DAPK siRNA (Control) failed to down-regulate DAPK mRNA. A reduction in DAPK protein level by DAPK siRNA was demonstrated by immunoblots (Fig. 3*B*). Quantitation by densitometer indicated a decrease of 68% in DAPK protein in DO11.10 cells expressing DAPK siRNA. This down-regulation of DAPK led to enhanced CD3/CD28-induced IL-2 production (Fig. 3*C*), as well as Ag-stimulated IL-2 generation (Fig. 3*D*) in DO11.10 cells. In contrast, nonspecific siRNA expression (Control, Fig. 3, *C* and *D*) did not affect T cell activation.

We knocked down DAPK in Jurkat T cells using two different siRNA sequences (si-1, si-2) specific for human DAPK (Fig. 3*E*). More than 80% of DAPK protein level was reduced by either DAPKsi-1 or DAPKsi-2 in Jurkat cells, in contrast to the nonspecific control siRNA. DAPK activity was measured in

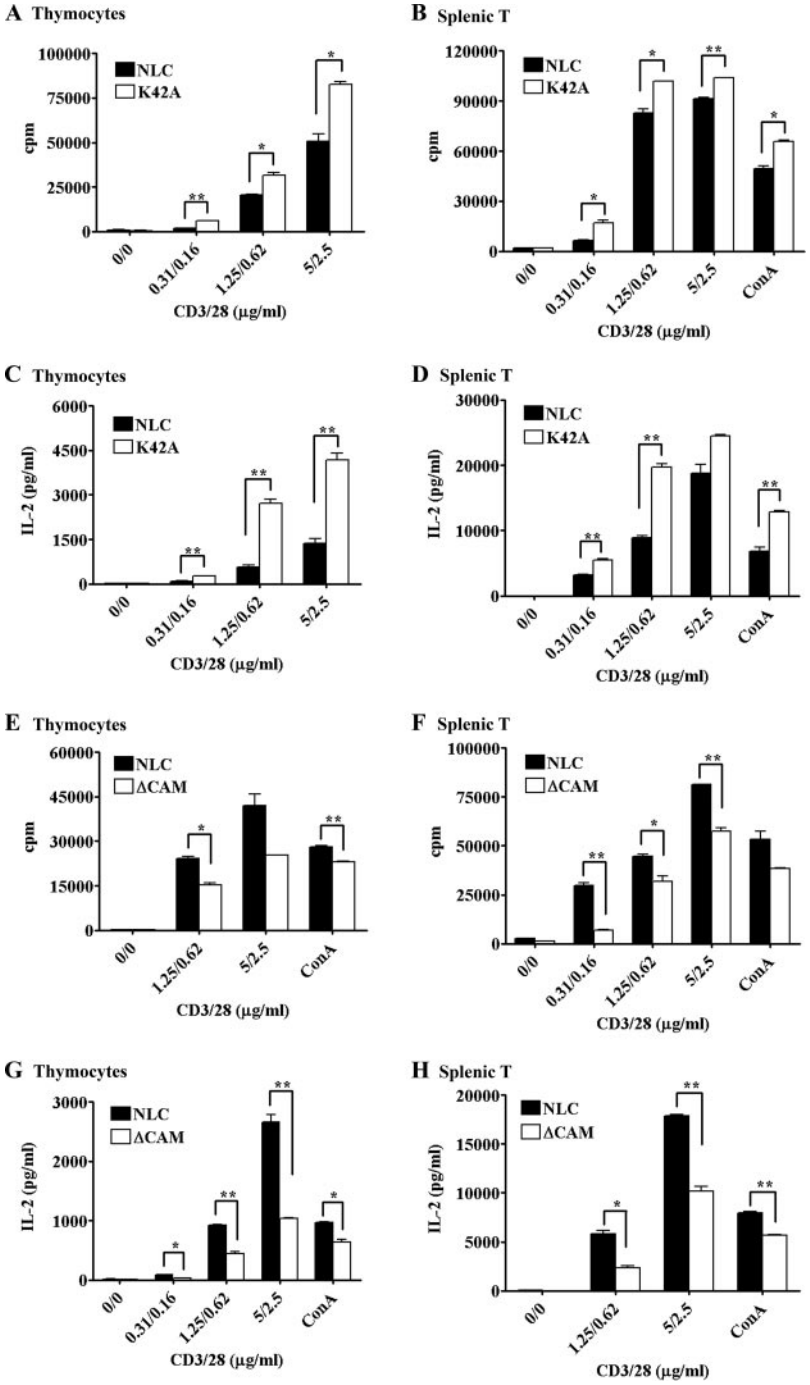

FIGURE 5. The [K42A]DAPK transgene enhances T cell proliferation and IL-2 production, while the [ΔCAM]DAPK transgene suppresses T cell proliferation and IL-2 generation. *A–D*, The [K42A]DAPK transgene increased TCR-activated T cell proliferation and IL-2 generation. Splenic T cells were isolated from splenocytes using anti-mouse Ig panning, and the purity of splenic T cells was >92%, determined by CD3 expression. Thymocytes (*A*) and purified splenic T cells (*B*) (4×10^5 cells/well) from NLC and CD2-[K42A]DAPK-transgenic mice were activated with indicated concentrations of immobilized anti-CD3 plus anti-CD28 Abs or Con A (5 μg/ml), and the incorporation of thymidine was determined 60 h later. IL-2 production from CD3/CD28-stimulated thymocytes (*C*) and splenic T cells (*D*) was quantitated 24 h later. *E–H*, [ΔCAM]DAPK transgene suppressed TCR-stimulated T cell proliferation and IL-2 production. Thymocytes (*E*) and splenic T cells (*F*) from NLC and CD2-[ΔCAM]DAPK-transgenic mice were activated as in *A* and T cell proliferation was determined 60 h later. IL-2 production from thymocytes (*G*) and splenic T cells (*H*) were quantitated 24 h after anti-CD3/anti-CD28 or Con A stimulation. *, $p < 0.05$; **, $p < 0.01$ for paired *t* test.

DAPK-knockdown Jurkat cells. MLC is the in vivo substrate of DAPK (3, 5, 17–19). In control Jurkat cells, TCR stimulation resulted in increased phosphorylation of MLC (Fig. 3*F*). Down-regulation of DAPK in Jurkat cells reduced MLC phosphorylation before TCR ligation, and impaired TCR-induced MLC phosphorylation. This result illustrates that DAPK physiological function was compromised in DAPK-knockdown T cells, and further supports that DAPK is involved in TCR-mediated MLC activation. Down-regulation of DAPK increased IL-2 production stimulated by CD3/CD28, while nonspecific siRNA had no effect on the activation of Jurkat cells (Fig. 3*G*). Therefore, specific down-regulation of DAPK leads to enhanced TCR-stimulated activation, supporting the role of endogenous DAPK as a negative regulator of T cell activation.

Transgenic [K42A]DAPK promotes T cell activation and transgenic [ΔCAM]DAPK suppresses T cell activation

Both DO11.10 and Jurkat are transformed T cells. To elucidate the function of DAPK in normal T cells, we generated transgenic mice with T cell-specific expression of [K42A]DAPK and [ΔCAM]DAPK. [K42A]DAPK and [ΔCAM]DAPK were expressed under CD2 promoter (Fig. 4*A*). Transgene expression was identified by PCR analysis of tail DNA and RT-PCR analysis of peripheral blood leukocytes (data not shown). Three independent transgenic mouse lines for each construct were used for T cell activation studies. Immunoblots illustrate the expression of DAPK in the three lines of transgenic mice (Tg-1, Tg-2, Tg-3) relative to a normal littermate control (NLC) for both [K42A]DAPK and [ΔCAM]DAPK

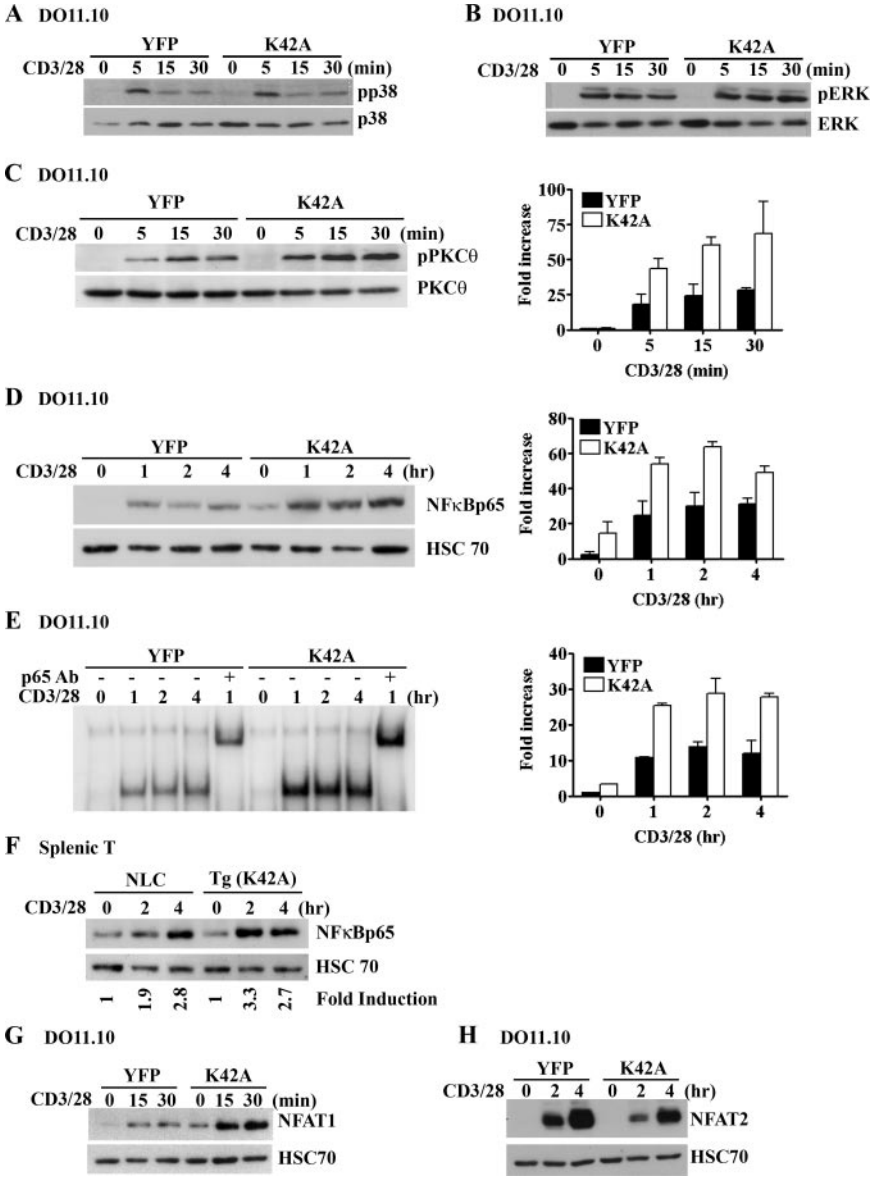

FIGURE 6. [K42A]DAPK enhances TCR-stimulated NF-κB activation. *A*, Activation of p38 MAPK was not affected by [K42A]DAPK. DO11.10 T cells expressing YFP vector or [K42A]DAPK were stimulated with immobilized anti-CD3 (5 μg/ml) and anti-CD28 (2.5 μg/ml) and total cellular extracts were prepared at the indicated time points. p38 MAPK activation was evaluated by anti-phospho-p38 MAPK Ab. *B*, [K42A]DAPK weakly enhanced TCR-induced ERK activation. ERK activation was determined on extracts prepared in *A*, using anti-phospho-ERK Ab. *C*, [K42A]DAPK increased TCR-induced PKCθ activation. PKCθ activation was determined on extracts prepared in *A* by anti-phospho-PKCθ (T538) Ab, using total lysate PKCθ as an internal control (*left panel*). The intensity of phospho-PKCθ was determined by densitometer, normalized against HSC70, and fold increase was calculated using the unstimulated YFP control as 1 (*right panel*). Data are the average of two independent studies. *D*, [K42A]DAPK enhanced TCR-stimulated NF-κB p65 nuclear translocation. DO11.10 T cells expressing YFP vector or [K42A]DAPK were stimulated as in *A*, and nuclear extracts were prepared at the indicated time points. NF-κB p65 was detected by immunoblot (*left panel*) and quantitated by densitometry as in *C* (*right panel*). *E*, [K42A]DAPK promoted the formation of NF-κB-DNA complex. DNA-binding activity of NF-κB in nuclear extracts prepared from *D* were evaluated by EMSA using labeled oligonucleotides containing the consensus κB sequence. The presence of p65 in the binding complex was illustrated by supershift with anti-p65 Ab. The quantities of the specific NF-κB-DNA complex was assessed and the fold increase shown in the *right panel.* Data are mean of two separated experiments. *F*, [K42A]DAPK transgene enhanced NF-κB activation in normal T cells. Splenic T cells from NLC and CD2-[K42A]DAPK-transgenic mice were stimulated with anti-CD3 (5 μg/ml) plus anti-CD28 (2.5 μg/ml), and the nuclear translocation of NFκB p65 was similarly determined. Numbers in the bottom indicate fold induction using the resting NLC T cells as 1. *G* and *H*, [K42A]DAPK increased the activation of NFAT1 but not NFAT2. YFP- and [K42A]DAPK-DO11.10 T cells were activated by CD3/CD28 and nuclear extracts prepared at the indicated time points. The presence of NFAT1 (*G*) and NFAT2 (*H*) were determined by immunoblots using Abs specific for NFAT1 and NFAT2, respectively.

(Fig. 4, *B* and *C*). DAPK has been shown to participate in apoptosis triggered by different stimuli (2, 6). Consistent with previous finding, [K42A]DAPK-transgenic thymocytes displayed a moderate but significant reduction in Fas-induced apoptosis (Fig. 4*D*) and DNA damage-mediated cell death (Fig. 4*F*). In contrast, [ΔCAM]DAPK-transgenic thymocytes were more sensitive to Fas-triggered cell death (Fig. 4*E*) and etoposide-induced apoptosis (Fig. 4*G*). We also tested susceptibility of [K42A]DAPK- and [ΔCAM]DAPK-transgenic thymocytes to TNF-α-induced cell death. Thymocytes were relatively resistant to TNF-α-triggered apoptosis (42). Cycloheximide (CHX) has to be included for death induction, yet CHX also led to a significant amount of background

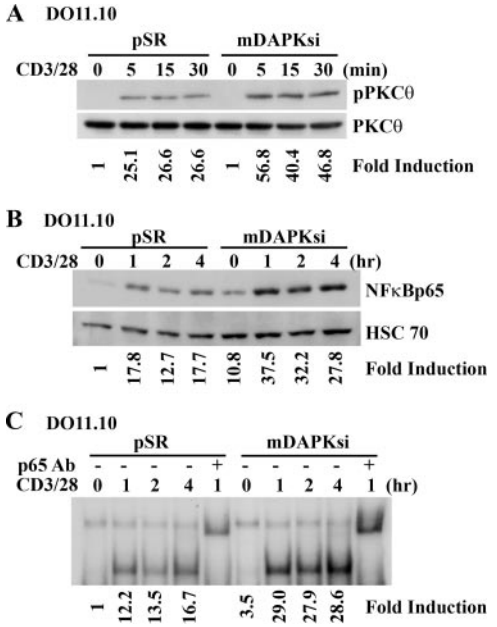

FIGURE 7. DAPK knockdown enhances TCR-stimulated NF-κB activation in DO11.10 T cells. *A*, Down-regulation of DAPK increased TCR-induced PKCθ activation. Vector control DO11.10 T cells (pSR) or DO11.10 cells with DAPK knockdown (mDAPKsi) were stimulated with immobilized anti-CD3 (5 μg/ml) and anti-CD28 (2.5 μg/ml) before determination of PKCθ phosphorylation. The contents of phospho-PKCθ were determined as in Fig. 6, and relative fold of induction was calculated using unstimulated pSR T cells as 1. *B*, DAPK knockdown enhanced TCR-stimulated NF-κB p65 nuclear translocation. Control and DAPK-knockdown DO11.10 cells were stimulated as in *A*, and nuclear appearance of NF-κB p65 was detected by immunoblot. Numbers are fold of induction. *C*, Down-regulation of DAPK promoted the formation of NF-κB-DNA complex. DNA-binding activity of NF-κB in nuclear extracts prepared from *B* were evaluated by EMSA. The presence of p65 in the binding complex was illustrated by supershift with anti-p65 Ab. Fold induction of the specific NF-κB-DNA complex is indicated at the *bottom*.

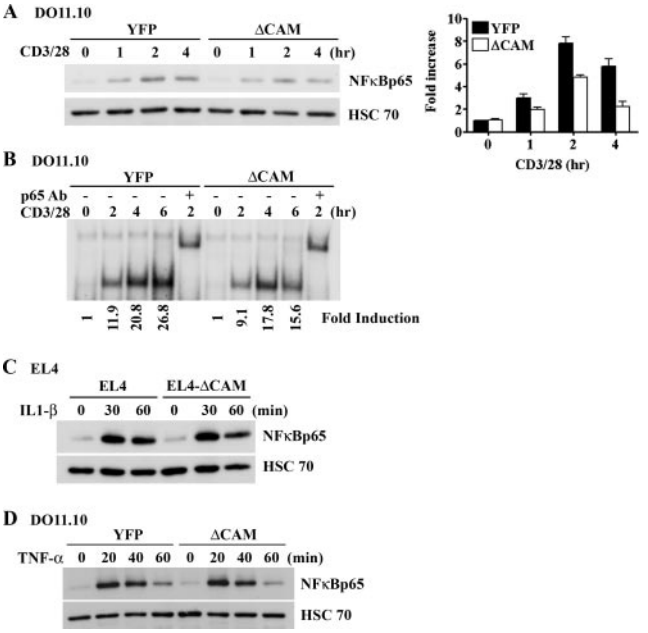

FIGURE 8. Active DAPK suppresses TCR-induced, but not IL-1β and TNF-α-triggered, NF-κB activation. *A* and *B*, [ΔCAM]DAPK inhibited TCR-induced NF-κB activation. DO11.10 T cells expressing YFP vector or ΔCAM were stimulated with anti-CD3 (0.5 μg/ml) and anti-CD28 (0.25 μg/ml), and nuclear extracts were prepared at the indicated time points. NF-κB p65 was detected by immunoblot (*A*) using NF-κB p65-specific Ab, and the DNA-binding activity of nuclear NF-κB was evaluated by EMSA (*B*). Relative increase of nuclear p65 from two independent experiments are displayed (*A*, *right panel*). Fold induction of the specific NF-κB-DNA complex is indicated at the *bottom* (*B*). *C* and *D*, DAPK did not affect IL-1β- and TNF-α-induced NF-κB activation. Control and [ΔCAM]DAPK-expressing EL4 (*C*) or DO11.10 cells (*D*) were stimulated with IL-1β (*C*) or TNF-α (*D*), and nuclear entry of p65 was measured at the time points indicated.

death (Fig. 4, *H* and *I*). Despite the high background, TNF-α-induced cell death was attenuated by expression of [K42A]DAPK transgene, and was increased by [ΔCAM]DAPK transgene. It may be noted that the modulatory effect of DAPK was more prominent in etoposide-triggered apoptosis than in Fas/TNF-α-induced cell death. Whether this suggests a more dominant role of DAPK in mitochondrial-mediated (intrinsic) apoptosis than death receptor-induced (extrinsic) cell death in T cells is being examined.

TCR-induced proliferation of thymocytes was higher in CD2-[K42A]DAPK-transgenic mice than in their NLC counterparts (Fig. 5*A*). Transgenic expression of [K42A]DAPK also promoted proliferation triggered by TCR and Con A in splenic T cells (Fig. 5*B*). A more prominent enhancement in TCR- or Con A-stimulated IL-2 production was found in thymocytes (Fig. 5*C*) and splenic T cells (Fig. 5*D*) from [K42A]DAPK-transgenic mice. Therefore, inhibition of DAPK by its DN form increased TCR-mediated T cell proliferation and IL-2 production in normal T cells.

In contrast, active DAPK transgene exhibited a suppressive effect on T cell activation. Proliferation of thymocytes, induced by CD3/CD28 or Con A, was significantly inhibited in [ΔCAM]DAPK-transgenic thymocytes, relative to NLC thymocytes (Fig. 5*E*). Reduced proliferation stimulated through TCR or Con A was also found in splenic T cells from [ΔCAM]DAPK-transgenic mice (Fig. 5*F*). The inhibitory effect of transgenic [ΔCAM]DAPK was also evident when measuring TCR- or Con A-stimulated IL-2 production in thymocytes (Fig. 5*G*) and in splenic T cells (Fig. 5*H*). Consistent with the stimulatory activity of [K42A]DAPK, constitutive DAPK activation in normal T cells suppresses TCR-induced activation.

DAPK targets to TCR-induced NF-κB activation

We examined various activation signals in T cells expressing DN-DAPK and active DAPK. Some of the signaling events, such as p38 MAPK activation, were not affected by DN-DAPK (Fig. 6*A*). ERK activation was slightly elevated in T cells expressing [K42A]DAPK (Fig. 6*B*). In addition to elevated ERK phosphorylation, inhibition of DAPK led to increased phosphorylation of PKCθ after TCR stimulation in T cells (Fig. 6*C*). Quantitation by densitometry indicates an at least 2-fold increase of TCR-induced PKCθ phosphorylation in [K42A]DAPK-expressing T cells. Because PKCθ is coupled to NF-κB activation, we then examined the status of NF-κB in T cells expressing [K42A]DAPK. In resting T cells expressing [K42A]DAPK, there was a small increase in nuclear translocation of NF-κB p65 (Fig. 6*D*). TCR stimulation resulted in nuclear appearance of NF-κB p65 in control cells, with a significant elevation in DO11.10 T cells expressing [K42A]DAPK. The [K42A]DAPK-mediated increase in nuclear p65 correlates well with the increase in phospho-PKCθ (Fig. 6*D*). The enhanced NF-κB p65 nuclear translocation in [K42A]DAPK T cells was accompanied with increased binding to κB DNA element revealed by EMSA (Fig. 6*E*). No κB DNA-binding complex was detected before T cell activation, despite the presence of nuclear p65 in resting [K42A]DAPK T cells. Stimulation with CD3/CD28 led to formation of the specific κB DNA-binding complex, as confirmed

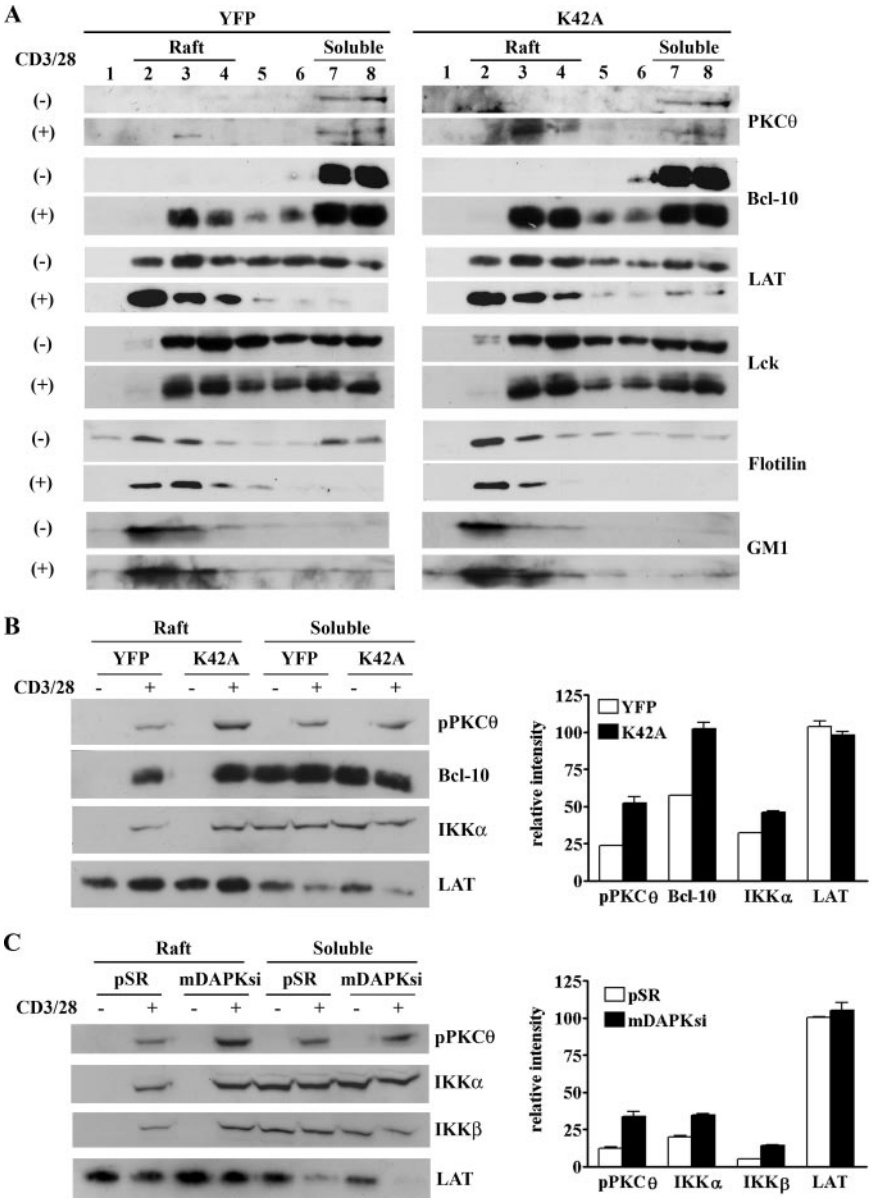

FIGURE 9. Inhibition or down-regulation of DAPK increases TCR-stimulated raft recruitment of pPKCθ, Bcl-10, and IKKα but not LAT. *A*, A total of 5×10^7 DO11.10 T cells expressing YFP vector or [K42A]DAPK were stimulated with immobilized anti-CD3 (5 μg/ml) and anti-CD28 (2.5 μg/ml) at 37°C for 30 min. The cells were lysed with 0.25% Triton X-100 and sucrose density gradient centrifugation was then used to separate lipid rafts from soluble fractions. Raft fractions (fractions 2–4) and soluble parts (fractions 7 and 8) were resolved on SDS-PAGE, and analyzed by immunoblot with Abs specific for PKCθ, Bcl-10, LAT, Lck, GM1, and flotillin. *B*, Raft fractions (fractions 2–4) and soluble parts (fractions 7 and 8) from *A* were pooled separately, resolved on SDS-PAGE, and analyzed by immunoblot with Abs specific for pPKCθ, Bcl-10, IKKα, and LAT. The relative amounts of pPKCθ, Bcl-10, IKKα, and LAT in raft fractions were quantitated by densitometry. Data are reported as means and SEs of three independent experiments (*right panel*). *C*, Increased partition of NF-κB-signaling molecules into rafts by DAPK knockdown. A total of 5×10^7 DO11.10 cells each of control or DAPK knockdown were stimulated with anti-CD3 (5 μg/ml) and anti-CD28 (2.5 μg/ml) at 37°C for 30 min. The cells were then lysed with 0.25% Triton X-100 and subjected to sucrose density gradient centrifugation to isolate lipid rafts. Raft fractions (fractions 2–4) and soluble parts (fractions 7 and 8) were pooled, separated through SDS-PAGE, and analyzed using immunoblot with Abs specific for pPKCθ, IKKα, IKKβ, and LAT. Quantitation of Raft-associated proteins were quantitated as in *B* and the relative intensity is shown in the *right panel*.

by the supershift by anti-p65 Ab (Fig. 6*E*). The amount of κB DNA-binding complex, quantitated by densitometer, in activated [K42A]DAPK-expressing DO11.10 cells was twice as much as that in activated YFP DO11.10 cells. The increased NF-κB activation mediated by [K42A]DAPK was also seen with normal T cells. In [K42A]DAPK-transgenic T cells, TCR triggered increased translocation of NF-κB p65. Together, these results suggest an inhibitory role of DAPK in NF-κB activation (Fig. 6*F*). The effect of [K42A]DAPK on NFAT1 activation, another major transcription factor stimulated by TCR, was as prominent as NF-κB. [K42A]DAPK expression led to a large increase in nuclear translocation of NFAT1 (Fig. 6*G*). However, DAPK exhibited an opposite effect on the activation of NFAT2. [K42A]DAPK moderately decreased the nuclear presence of NFAT2 (Fig. 6*H*).

To further delineate the link between DAPK and NF-κB, the activation of NF-κB was examined in T cells with specific knockdown of DAPK. This down-regulation of DAPK led to an elevation of TCR-induced phospho-PKCθ (Fig. 7*A*). Densitometry indicates that DAPK knockdown resulted in a nearly 2-fold increase in PKCθ phosphorylation. Down-regulation of DAPK also resulted in nuclear appearance of p65 before T cell activation (Fig. 7*B*), similar to that seen in [K42A]DAPK T cells (Fig. 6*D*). NF-κB p65 nuclear entry stimulated by CD3/CD28 increased by 100% in DAPK-depleted T cells relative to control T cells. The enhanced formation of NF-κB-DNA complex in T cells with down-regulated DAPK was further demonstrated by EMSA (Fig. 7*C*). These results support the specificity of DAPK on NF-κB inhibition.

The possible antagonism of NF-κB activation by DAPK was also examined in T cells expressing active DAPK. Fig. 8*A* illustrates that TCR-induced nuclear translocation of NF-κB p65 was attenuated in DO11.10 T cells expressing [ΔCAM]DAPK. Quantitation from two independent experiments illustrates a clear reduction in nuclear entry of p65 in T cells with active DAPK (Fig. 8*A*, *right panel*). This was consistent with the reduced formation of κB DNA-binding complex when [ΔCAM]DAPK T cells were activated (Fig. 8*B*). Therefore, TCR-mediated NF-κB activation is negatively regulated by DAPK.

DAPK does not affect NF-κB activation stimulated by TNF-α or IL-1β

NF-κB is stimulated by TNF-α and IL-1β in cascades distinct from that activated by TCR (25, 32, 33). We further examined

whether NF-κB activation stimulated through TCR-independent pathways was similarly regulated by DAPK. T cells were treated with IL-1β to stimulate NF-κB activation. We used EL4 T cells for this study as DO11.10 cells were not responsive to IL-1β. Fig. 7*C* illustrates that expression of [ΔCAM]DAPK in EL4 cells did not alter IL-1-stimulated NF-κB activation. We also examined the effect of DAPK on TNF-α-triggered NF-κB activation. NF-κB was activated in DO11.10 cells immediately followed the treatment with TNF-α (Fig. 8*D*). Expression of [K42A]DAPK did not affect the nuclear entry of p65 induced by TNF-α. Therefore, DAPK does not modulate NF-κB activation stimulated by TNF-α or IL-1β, DAPK specifically regulates TCR-induced NF-κB activation.

Inhibition of DAPK increases the entry of PKCθ, Bcl-10, and IKKα into membrane rafts

The enhanced activation of PKCθ by [K42A]DAPK or DAPK-specific siRNA suggests that DAPK acts at a step before IKK activation in the TCR-induced NF-κB activation pathway. TCR-induced activation signals lead to the assembly of the phospho-PKCθ, caspase recruitment domain-11-Bcl10-MALT1 complex, and the IKK complex on membrane rafts (27–32). We evaluated the association of these NF-κB-activating molecules with membrane rafts after TCR stimulation. Lipid rafts were separated from soluble fractions by centrifuge on sucrose gradient. Fig. 8*A* illustrates a typical profile on the distribution of PKCθ, Bcl-10, Lck, and raft markers flotillin and GM-1 in membrane raft fractions and soluble fractions before and after TCR stimulation. In unstimulated T cells, PKCθ and Bcl-10 were located mainly in the soluble fractions, while LAT and Lck were present in both soluble and raft fractions (Fig. 9*A*). TCR stimulation induced distribution of PKCθ and Bcl-10 into raft fractions, resulting in their appearance in both raft and soluble fractions (Fig. 9*A*). For LAT, CD3/CD28 ligation triggered its translocation from soluble fractions into lipid rafts, leading to a clear reduction of LAT in soluble fractions. In contrast, Lck distribution among raft and soluble fractions was not changed before and after TCR engagement (Fig. 9*A*). TCR-induced raft localization of Bcl-10 and PKCθ was increased in [K42A]DAPK-expressing cells relative to the YFP control, while TCR-mediated raft localization of LAT was not significantly affected by [K42A]DAPK expression (Fig. 9*A*). For ease of comparison, raft fractions and soluble fractions were pooled separately for analysis of the signaling protein contained (Fig. 9*B*). In CD3/CD28-stimulated T cells, inactivation of DAPK by expression of [K42A]DAPK resulted in an increase of phospho-PKCθ, Bcl-10, and IKKα in membrane rafts (Fig. 9*B*). Densitometer measurement of protein quantities from three independent experiments (Fig. 9*B*, *right panel*) also illustrate the enhanced raft distribution of phospho-PKCθ, Bcl-10, and IKKα in [K42A]DAPK T cells. In contrast, distribution of LAT in the membrane raft fraction was not altered in activated [K42A]DAPK T cells (Fig. 9*B*). Regulation of raft localization of NF-κB-activating molecules by DAPK was further confirmed in T cells with DAPK knockdown. Fig. 9*C* illustrates a similar enhanced partition of phospho-PKCθ, IKKα, and IKKβ into the raft in activated DO11.10 T cells with down-regulated DAPK. Quantitation analysis from two independent experiments supports the notion that TCR-induced raft localization of phospho-PKCθ, IKKα, and IKKβ was enhanced in DAPK-knockdown cells (Fig. 9*C*, *right panel*). Therefore, inhibition of DAPK by [K42A]DAPK or DAPK knockdown by siRNA increases the localization of NF-κB-activating molecules into membrane raft after T cell activation.

Discussion

In the present study, through the use of active DAPK, DN DAPK, and DAPK-specific siRNA, DAPK was found to antagonize T cell activation. Our results clearly illustrate that DAPK and [ΔCaM]DAPK suppressed T cell activation in both T cell lines and normal T cells, while inhibition of DAPK by [K42A]DAPK or down-regulation by siRNA increases T cell proliferation and IL-2 production (Figs. 2, 3, and 5). We further mapped one of the T cell signals specifically suppressed by DAPK to NF-κB activation (Figs. 6–8). The entry of NF-κB-activating molecules, including PKCθ, Bcl-10, and IKK, into membrane rafts after TCR ligation was enhanced when DAPK was suppressed or knocked down (Fig. 9). NF-κB, therefore, represents a novel target of DAPK in T cells.

DAPK has not been shown to be involved in T cell activation. In this study, we have first demonstrated an immediate activation of DAPK after TCR engagement (Fig. 1*A*). The activation of DAPK lasted for ~2 h and then became gradually inactivated, shown by rephosphorylation of DAPK at serine 208 (Fig. 1*B*). Additional evidence of a direct participation of DAPK in T cell activation is shown by the phosphorylation of MLC. DAPK directly phosphorylates MLC (4, 43). TCR stimulation led to increased phosphorylation of MLC, while DAPK knockdown impaired MLC phosphorylation (Fig. 3*F*), supporting a contribution of DAPK activity to TCR-triggered MLC phosphorylation. From the time course of DAPK activation, the major targets of DAPK are likely those molecules that participated in the earlier phase (<90 min) of T cell activation. The molecular processes involved in DAPK activation and inactivation remain to be characterized in T cells. The phosphatase that is responsible for dephosphorylation of DAPK at Ser^{308} is still unknown (3). Even though DAPK is autophosphorylated at Ser^{308}, we have not identified the exact signaling molecule that initiates DAPK inactivation processes during late T cell activation.

Another finding on DAPK during T cell activation is the decrease in the DAPK protein levels at later time points (>4 h) following TCR stimulation (Fig. 1*B*). DAPK protein stability is regulated by several distinct mechanisms (40, 41, 44–47). Dephosphorylation at Ser^{308} and activation of DAPK by TNF-α, ceramide, or ischemia results in DAPK degradation (40, 41). The binding of DAPK to DAPK-interacting protein-1, an E3 ubiquitin ligase, is reported to promote proteolysis of DAPK by proteasome (44, 46). The interaction of DAPK with cathepsin B prevents the degradation of DAPK (47). DAPK is also stabilized by Hsp90 and, in the absence of Hsp90, becomes susceptible to DIP-1- and carboxyl terminus of HSC70-interacting protein-mediated ubiquitination (45, 46). In the present study, DAPK was found degraded followed the initial activation, yet Ser^{308} phosphorylation was reintroduced before extensive DAPK destabilization (Fig. 1*B*). This may somewhat distinguish TCR-induced DAPK degradation from ischemia/ceramide-triggered DAPK down-regulation (40, 41). Delineation on how TCR activation signals regulate the stability of DAPK protein shall help understand the dynamic turnover of DAPK protein in activated T cells and its physiological impact.

A distant DAPK-related kinase, DRAK2, has been characterized for its function in T lymphocytes. DAPK shares 51% identify in kinase domain with DRAK2, yet DRAK2 lacks all the DAPK domains that are 3′ to kinase domain. Transgenic expression of DRAK2 results in enhanced T cell apoptosis and increased IL-2 production, but does not affect T cell proliferation (48). This is in contrast to the suppression of IL-2 production and reduced T cell proliferation observed in [ΔCAM]DAPK-transgenic mice (Fig. 5, *E–H*). Deficiency in DRAK2 leads to elevated T cell proliferation

and IL-2 production (49), similar to those found in [K42A]DAPK-transgenic mice (Fig. 5, *A–D*). However, [K42A]DAPK-transgenic T cells displayed specific augmentation in NF-κB activation (Fig. 6), which was not observed in DRAK2^{null} T cells (49). Therefore, DAPK and DRAK2, which are two distinct members of DAPK family, display different physiological roles in T cell activation.

Another important finding of the present study is that DAPK regulates NF-κB activation induced by TCR, but not by TNF-α and IL-1β (Fig. 8, *C* and *D*). A previous report has shown that TNF-α-induced NF-κB activation was not affected by [K42A]DAPK in HeLa cells (16). In the present study, we identified the stage of NF-κB activation targeted by DAPK to be at or before PKCθ activation (Fig. 6), operated specifically for TCR-induced NF-κB activation, but not in TNF-α- or IL-1-triggered NF-κB activation (27, 34, 35). This explains why TNF-α- or IL-1-triggered NF-κB activation is not sensitive to action of DAPK. The other type of receptor known to activate NF-κB through PKCθ is B cell Ag receptor. Based on results from this study, we may predict that DAPK inhibits NF-κB activation in B cells stimulated through their Ag receptor, similar to that observed in T cells. Our observation that DAPK does not modulate NF-κB activation induced by Ag receptor-independent pathways in T lymphocytes (Fig. 6) also suggests that DAPK is unlikely to affect NF-κB activation in nonlymphocytes.

TCR ligation leads to localization of TCR and signaling molecules in lipid rafts for the assembly of TCR-signaling complexes containing lck, CD3, LAT, and PKCθ (28, 50–52). Recent studies illustrate that TCR activation leads to the assembly of phospho-PKCθ, the caspase recruitment domain-11-Bcl10-MALT1 complex, and the IKK complex into membrane rafts (28–33). By use of [K42A]DAPK to inhibit DAPK activation or siRNA to down-regulate DAPK, the localization of PKCθ, Bcl10, and IKK in the membrane raft fraction was increased (Fig. 9). TCR-stimulated lipid raft formation involves reorganization of actin cytoskeletons (51, 52). It may be postulated that DAPK, known to have a profound effect on the cytoskeleton, regulates the gathering of membrane rafts and consequently, activation of NF-κB.

In addition to phospho-PKCθ, other signaling molecules such as LAT are known to relocate into the raft fraction after TCR stimulation. We did not find any effect of DAPK on the raft entry of LAT (Fig. 9). The inhibitory effect of DAPK on the translocation of PKCθ, but not LAT, into lipid rafts indicates specificity of DAPK for the NF-κB-activating complex. The molecular mechanism underlying this discriminative effect of DAPK is currently unclear. There is a possibility that membrane rafts are heterogeneous with regard to their content of the NF-κB-activating complex and LAT. Because raft formation involves cytoskeleton reorganization, DAPK may target cytoskeleton that affects the raft-embedding NF-κB-activating complex. Alternatively, DAPK may target some molecules upstream of PKCθ, resulting in reduced phosphorylation of CARD-containing membrane associated guanylated kinase protein1 and impaired assembly of the NF-κB-activating complex on rafts (33). A few signaling molecules, including IL-1R-associated kinase 4 and 3-phosphoinositide-dependent kinase1, have recently been shown to mediate TCR-induced activation of PKCθ/IKK (32, 53). Further examination of whether DAPK interacts with these molecules or modulates their activation may aid in our understanding the exact stage at which DAPK intercepts NF-κB activation in T cells, and may help unveil additional molecular processes along the TCR-stimulated NF-κB activation pathway.

The specific activation of DAPK lasted for 90 min after TCR stimulation (Fig. 1*A*), DAPK was then inactivated before extensive degradation in T cells (Fig. 1*B*). The T cell-signaling molecules that are regulated by DAPK are likely restricted to those that are activated before 90 min. We found that TCR-induced activation of NFAT1 was enhanced when DAPK was inhibited by [K42A]DAPK, yet activation of NFAT2 was attenuated in the presence of [K42A]DAPK (Fig. 6, *G* and *H*). TCR ligation leads to immediate dephosphorylation and translocation of NFAT1 into the nucleus (54), while NFAT2 activation requires transcription, new protein synthesis, and nuclear entry (55). Nuclear presence of NFAT2 peaked 4 h after TCR stimulation (Fig. 6, *G* and *H*). We suggest that the differential effect of DAPK on the activation of NFAT1 and NFAT2 is likely due to the difference in the activation kinetics between NFAT1 and NFAT2. Therefore, NFAT1, like two other early T cell activation molecules, PKCθ and ERK, is negatively regulated by DAPK (Fig. 6). In contrast, NFAT2, with full activation 4 h after TCR stimulation, is much less dependent on DAPK. A small decrease in NFAT2 activation when DAPK was inhibited (Fig. 6*H*) could be due to requirement of multiple distinct steps in NFAT2 activation (55), that one of the steps may be positively regulated by DAPK. Further study will help delineate the molecular process of NFAT2 activation in which DAPK participates.

DAPK is a serine/threonine kinase with multiple domains and participates in many forms of apoptosis. We found that Fas-triggered and DNA damage-induced apoptosis were attenuated in [K42A]DAPK-transgenic thymocytes and elevated in [ΔCAM]DAPK-transgenic thymocytes (Fig. 4, *D* and *E*). Previous studies have illustrated several mechanisms that contribute to the proapoptotic effect of DAPK. In the present study, we suggest a further possibility that inhibition of NF-κB, a major antiapoptotic molecule, contributes to apoptosis induction in T cells. NF-κB activates the expression of numerous antiapoptotic proteins, such as c-IAP-1, c-IAP-2, A20, and cellular FLIP. The ability of DAPK to inhibit NF-κB therefore suggests another physiological activity that adds to the proapoptotic effect of DAPK by down-regulation of antiapoptotic molecules in T cells. Our studies reveal for the first time the critical role of tumor suppressor DAPK in T cell activation. Further investigation shall help delineate the exact participation of DAPK in T cell immune responses, T cell tolerance, and T cell development.

Acknowledgments

We thank Drs. Leo Chi-Kwang Wang and Si-Tse Jiang for the production of transgenic mice, Dr. Dimitris Kioussis for the human CD2 cassette, Dr. Gina Costa for PGC-IRES-YFP, Dr. Garry Nolan for Phoenix and Eco-Jurkat cells, and Dr. Shie-Liang Hsieh for providing human T cells.

Disclosures

The authors have no financial conflict of interest.

References

1. Shohat, G., G. Shani, M. Eisenstein, and A. Kimchi. 2002. The DAP-kinase family of proteins: study of a novel group of calcium-regulated death-promoting kinases. *Biochim. Biophys. Acta* 1600: 45–50.
2. Bialik, S., and A. Kimchi. 2004. DAP-kinase as a target for drug design in cancer and diseases associated with accelerated cell death. *Semin. Cancer Biol.* 14: 283–294.
3. Bialik, S., and A. Kimchi. 2006. The death-associated protein kinases: structure, function, and beyond. *Annu. Rev. Biochem.* 75: 189–210.
4. Cohen, O., E. Feinstein, and A. Kimchi. 1997. DAP-kinase is a Ca^{2+}/calmodulin-dependent, cytoskeletal-associated protein kinase, with cell death-inducing functions that depend on its catalytic activity. *EMBO J.* 16: 998–1008.
5. Deiss, L. P., E. Feinstein, H. Berissi, O. Cohen, and A. Kimchi. 1995. Identification of a novel serine/threonine kinase and a novel 15-kD protein as potential mediators of the γ interferon-induced cell death. *Genes Dev.* 9: 15–30.
6. Cohen, O., B. Inbal, J. L. Kissil, T. Raveh, H. Berissi, T. Spivak-Kroizaman, E. Feinstein, and A. Kimchi. 1999. DAP-kinase participates in TNF-α- and Fas-induced apoptosis and its function requires the death domain. *J. Cell Biol.* 146: 141–148.
7. Jang, C. W., C. H. Chen, C. C. Chen, J. Y. Chen, Y. H. Su, and R. H. Chen. 2002. TGF-β induces apoptosis through Smad-mediated expression of DAP-kinase. *Nat. Cell Biol.* 4: 51–58.

8. Pelled, D., T. Raveh, C. Riebeling, M. Fridkin, H. Berissi, A. H. Futerman, and A. Kimchi. 2002. Death-associated protein (DAP) kinase plays a central role in ceramide-induced apoptosis in cultured hippocampal neurons. *J. Biol. Chem.* 277: 1957–1961.
9. Yamamoto, M., T. Hioki, T. Ishii, S. Nakajima-Iijima, and S. Uchino. 2002. DAP kinase activity is critical for C_2-ceramide-induced apoptosis in PC12 cells. *Eur. J. Biochem.* 269: 139–147.
10. Wang, W. J., J. C. Kuo, C. C. Yao, and R. H. Chen. 2002. DAP-kinase induces apoptosis by suppressing integrin activity and disrupting matrix survival signals. *J. Cell Biol.* 159: 169–179.
11. Inbal, B., O. Cohen, S. Polak-Charcon, J. Kopolovic, E. Vadai, L. Eisenbach, and A. Kimchi. 1997. DAP kinase links the control of apoptosis to metastasis. *Nature* 390: 180–184.
12. Shang, T., J. Joseph, C. J. Hillard, and B. Kalyanaraman. 2005. Death-associated protein kinase as a sensor of mitochondrial membrane potential: role of lysosome in mitochondrial toxin-induced cell death. *J. Biol. Chem.* 280: 34644–34653.
13. Llambi, F., F. Calheiros-Lourenço, D. Gozuacik, C. Guix, L. Pays, G. Del Rio, A. Kimchi, and P. Mehlen. 2005. The dependence receptor UNC5H2 mediates apoptosis through DAP-kinase. *EMBO J.* 24: 1192–1201.
14. Stevens, C., Y. Lin, M. Sanchez, E. Amin, E. Copson, H. White, V. Durston, D. M. Eccles, and T. Hupp. 2007. A germ line mutation in the death domain of DAPK-1 inactivates ERK-induced apoptosis. *J. Biol. Chem.* 282: 13791–13803.
15. Raveh, T., and A. Kimchi. 2001. DAP kinase-a proapoptotic gene that functions as a tumor suppressor. *Exp. Cell Res.* 264: 185–192.
16. Raveh, T., G. Droguett, M. S. Horwitz, R. A. DePinho, and A. Kimchi. 2001. DAP kinase activates a $p19^{ARF}$/p53-mediated apoptotic checkpoint to suppress oncogenic transformation. *Nat. Cell Biol.* 3: 1–7.
17. Jin, Y., E. K. Blue, S. Dixon, L. Hou, R. B. Wysolmerski, and P. J. Gallagher. 2001. Identification of a new form of death-associated protein kinase that promotes cell survival. *J. Biol. Chem.* 276: 39667–39678.
18. Kuo, J. C., J. R. Lin, J. M. Staddon, H. Hosoya, and R. H. Chen. 2003. Uncoordinated regulation of stress fibers and focal adhesions by DAP kinase. *J. Cell Sci.* 116: 4777–4790.
19. Bialik, S., A. R. Bresnick, and A. Kimchi. 2004. DAP-kinase-mediated morphological changes are localization dependent and involve myosin-II phosphorylation. *Cell Death Differ.* 11: 631–644.
20. Murata-Hori, M., F. Suizu, T. Iwasaki, A. Kikuchi, and H. Hosoya. 1999. ZIP kinase identified as a novel myosin regulatory light chain kinase in HeLa cells. *FEBS Lett.* 451: 81–84.
21. Kuo, J. C., W. J. Wang, C. C. Yao, P. R. Wu, and R. H. Chen. 2006. The tumor suppressor DAPK inhibits cell motility by blocking the integrin-mediated polarity pathway. *J. Cell Biol.* 172: 619–631.
22. Chen, C. H., W. J. Wang, J. C. Kuo, H. C. Tsai, J. R. Lin, Z. F. Chang, and R. H. Chen. 2005. Bidirectional signals transduced by DAPK-ERK interaction promote the apoptotic effect of DAPK. *EMBO J.* 24: 294–304.
23. Anjum, R., P. P. Roux, B. A. Ballif, S. P. Gygi, and J. Blenis. 2005. The tumor suppressor DAP kinase is a target of RSK-mediated survival signaling. *Curr. Biol.* 15: 1762–1767.
24. Karin, M., and A. Lin. 2002. NF-κB at the crossroads of life and death. *Nat. Immunol.* 3: 221–227.
25. Voll, R. E., E. Jimi, R. J. Phillips, D. F. Barber, M. Rincon, A. C. Hayday, R. A. Flavell, and S. Ghosh. 2000. NF-κB activation by the pre-T cell receptor serves as a selective survival signal in T lymphocyte development. *Immunity* 13: 677–689.
26. Schmidt-Supprian, M., G. Courtois, J. Tian, A. J. Coyle, A. Israel, K. Rajewsky, and M. Pasparakis. 2003. Mature T cells depend on signaling through the IKK complex. *Immunity* 19: 377–389.
27. Siebenlist, U., Brown, K., and Claudio, E. 2005. Control of lymphocyte development by nuclear factor-κB. *Nat. Rev. Immunol.* 5: 435–445.
28. Bi, K., Y. Tanaka, N. Coudronniere, K. Sugie, S. Hong, M. J. van Stipdonk, and A. Altman. 2001. Antigen-induced translocation of PKC-θ to membrane rafts is required for T cell activation. *Nat. Immunol.* 2:556–563.
29. Thome, M., and J. Tschopp. 2003. TCR-induced NF-κB activation: a crucial role for Carma1, Bcl10 and MALT1. *Trends Immunol.* 24: 419–424.
30. Wang, D., R. Matsumoto, Y. You, T. Che, X. Y. Lin, S. L. Gaffen, and X. Lin. 2004. CD3/CD28 costimulation-induced NF-κB activation is mediated by recruitment of protein kinase C-θ, Bcl10, and IκB kinase β to the immunological synapse through CARMA1. *Mol. Cell. Biol.* 24: 164–171.
31. Weil, R., and A. Israel. 2006. Deciphering the pathway from the TCR to NF-κB. *Cell Death Diff.* 13: 826–833.
32. Lee, K. Y., F. D'Acquisto, M. S. Hayden, J. H. Shim, and S. Ghosh. 2005. PDK1 nucleates T cell receptor-induced signaling complex for NF-κB activation. *Science* 308: 114–118.
33. Matsumoto, R., D. Wang, M. Blonska, H. Li, M. Kobayashi, B. Pappu, Y. Chen, D. Wang, and X. Lin. 2005. Phosphorylation of CARMA1 plays a critical role in T cell receptor-mediated NF-κB activation. *Immunity* 23: 575–585.
34. Hayden, M. S., and S. Ghosh. 2004. Signaling to NF-κB. *Genes Dev.* 18: 2195–2224.
35. Chen, Z. J. 2005. Ubiquitin signaling in the NF-κB pathway. *Nat. Cell Biol.* 7: 758–765.
36. Shimonkevitz, R., J. Kappler, P. Marrack, and H. Grey. 1983. Antigen recognition by H-2-restricted T cells. I. Cell-free antigen processing. *J. Exp. Med.* 158: 303–316.
37. Nicoletti, I., G. Migliorati, M. C. Pagliacci, F. Grignani, and C. Riccardi. 1991. A rapid and simple method for measuring thymocyte apoptosis by propidium iodide staining and flow cytometry. *J. Immunol. Methods* 139: 271–279.
38. Zhumabekov, T., P. Corbella, M. Tolaini, and D. Kioussis. 1995. Improved version of a human CD2 minigene based vector for T cell-specific expression in transgenic mice. *J. Immunol. Methods* 185: 133–140.
39. Shohat, G., T. Spivak-Kroizman, O. Cohen, S. Bialik, G. Shani, H. Berrisi, M. Eisenstein, and A. Kimchi. 2001. The pro-apoptotic function of death-associated protein kinase is controlled by a unique inhibitory autophosphorylation-based mechanism. *J. Biol. Chem.* 276: 47460–47467.
40. Jin, Y., E. K. Blue, and P. J. Gallagher. 2006. Control of death-associated protein kinase (DAPK) activity by phosphorylation and proteasomal degradation. *J. Biol. Chem.* 281: 39033–39040.
41. Shamloo, M., L. Soriano, T. Wieloch, K. Nikolich, R. Urfer, R., and D. Oksenberg. 2005. Death-associated protein kinase is activated by dephosphorylation in response to cerebral ischemia. *J. Biol. Chem.* 280: 42290–42299.
42. Chau, B. N., T. T. Chen, Y. Y. Wan, J. DeGregori, and J. Y. Wang. 2004. Tumor necrosis factor α-induced apoptosis requires p73 and c-ABL activation downstream of RB degradation. *Mol. Cell. Biol.* 24: 4438–4447.
43. Shani, G., L. Marash, D. Gozuacik, S. Bialik, L. Teitelbaum, G. Shohat, and A. Kimchi. 2004. Death-associated protein kinase phosphorylates ZIP kinase, forming a unique kinase hierarchy to activate its cell death functions. *Mol. Cell. Biol.* 24: 8611–8626.
44. Jin, Y., E. K. Blue, S. Dixon, Z. Shao, and P. J. Gallagher. 2002. A death-associated protein kinase (DAPK)-interacting protein, DIP-1, is an E3 ubiquitin ligase that promotes tumor necrosis factor-induced apoptosis and regulates the cellular levels of DAPK. *J. Biol. Chem.* 277: 46980–46986.
45. Citri, A., D. Harari, G. Shohat, P. Ramakrishnan, J. Gan, S. Lavi, M. Eisenstein, A. Kimchi, D. Wallach, S. Pietrokovski, and Y. Yarden. 2006. Hsp90 recognizes a common surface on client kinases. *J. Biol. Chem.* 281: 14361–14369.
46. Zhang, L., K. P. Nephew, and P. J. Gallagher. 2007. Regulation of death-associated protein kinase: stabilization by HSP90 heterocomplexes. *J. Biol. Chem.* 282: 11795–11804.
47. Lin, Y., C. Stevens, and T. Hupp. 2007. Identification of a dominant negative functional domain on DAPK-1 that degrades DAPK-1 protein and stimulates TNFR-1-mediated apoptosis. *J. Biol. Chem.* 282: 16792–16802.
48. Mao, J., X. Qiao, H. Luo, and J. Wu. 2006. Transgenic drak2 overexpression in mice leads to increased T cell apoptosis and compromised memory T cell development. *J. Biol. Chem.* 281: 12587–12595.
49. McGargill, M. A., B. G. Wen, C. M. Walsh, and S. M. Hedrick. 2004. A deficiency in Drak2 results in a T cell hypersensitivity and an unexpected resistance to autoimmunity. *Immunity* 21: 781–791.
50. Zhang, W., R. P. Trible, and L. E. Samelson. 1998. LAT palmitoylation: its essential role in membrane microdomain targeting and tyrosine phosphorylation during T cell activation. *Immunity* 9: 239–246.
51. Dykstra, M., A. Cherukuri, H. W. Sohn, S. J. Tzeng, and S. K. Pierce. 2003. Location is everything: lipid rafts and immune cell signaling. *Annu. Rev. Immunol.* 21: 457–481.
52. He, H. T., A. Lellouch, and D. Marguet. 2005. Lipid rafts and the initiation of T cell receptor signaling. *Semin. Immunol.* 17: 23–33.
53. Suzuki, N., S. Suzuki, D. G. Millar, M. Unno, H. Hara, T. Calzascia, S. Yamasaki, T. Yokosuka, N. J. Chen, A. R. Elford, et al. 2006. A critical role for the innate immune signaling molecule IRAK-4 in T cell activation. *Science* 311: 1927–1932.
54. Loh, C., J. A. Carew, J. Kim, P. G. Hogan, and A. Rao. 1996. T-cell receptor stimulation elicits an early phase of activation and a later phase of deactivation of the transcription factor NFAT1. *Mol. Cell. Biol.* 16: 3945–3954.
55. Wu, C. C., S. C. Hsu, H. M. Shih, and M. Z. Lai. 2003. NFATc is a target of p38 mitogen activated protein kinase in T cells. *Mol. Cell. Biol.* 23: 8442–6454.